

See discussions, stats, and author profiles for this publication at: <https://www.researchgate.net/publication/261880559>

Revealing the Atomic Restructuring of Pt-Co Nanoparticles

ARTICLE *in* NANO LETTERS · APRIL 2014

Impact Factor: 13.59 · DOI: 10.1021/nl500553a · Source: PubMed

CITATIONS

21

READS

138

11 AUTHORS, INCLUDING:



[Huolin L Xin](#)

Brookhaven National Laboratory

95 PUBLICATIONS 1,936 CITATIONS

[SEE PROFILE](#)



[Eric Andrew Stach](#)

Brookhaven National Laboratory

392 PUBLICATIONS 15,672 CITATIONS

[SEE PROFILE](#)



[Lin-Wang Wang](#)

Lawrence Berkeley National Laboratory

336 PUBLICATIONS 10,977 CITATIONS

[SEE PROFILE](#)



[Haimei Zheng](#)

Lawrence Berkeley National Laboratory

59 PUBLICATIONS 2,221 CITATIONS

[SEE PROFILE](#)

Revealing the Atomic Restructuring of Pt–Co Nanoparticles

Huolin L. Xin,[†] Selim Alayoglu,^{†,‡} Runzhe Tao,[†] Arda Genc,[§] Chong-Min Wang,^{||} Libor Kovarik,^{||} Eric A. Stach,[†] Lin-Wang Wang,[†] Miquel Salmeron,^{†,¶} Gabor A. Somorjai,^{†,‡} and Haimei Zheng^{†,||,*}

[†]Materials Sciences Division, Lawrence Berkeley National Laboratory, Berkeley, California 94720 United States

[‡]Department of Chemistry, University of California, Berkeley, California 94720, United States

[§]FEI Company, 5350 NE Dawson Creek Drive, Hillsboro, Oregon 97124, United States

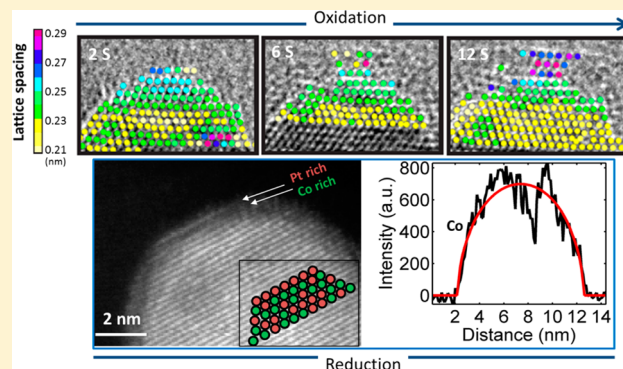
^{||}Environmental Molecular Sciences Laboratory, Pacific Northwest National Laboratory, P.O. Box 999, Richland, Washington 99352, United States

[¶]Center for Functional Nanomaterials, Brookhaven National Laboratory, Upton, New York 11973 United States

[¶]Department of Material Science and Engineering, University of California, Berkeley, California 94720 United States

S Supporting Information

ABSTRACT: We studied Pt–Co bimetallic nanoparticles during oxidation in O₂ and reduction in H₂ atmospheres using an aberration corrected environmental transmission electron microscope. During oxidation Co migrates to the nanoparticle surface forming a strained epitaxial CoO film. It subsequently forms islands via strain relaxation. The atomic restructuring is captured as a function of time. During reduction cobalt migrates back to the bulk, leaving a monolayer of platinum on the surface.



KEYWORDS: Catalysis, environmental TEM, *in situ* TEM, strain mapping, atomic-resolution TEM

Many bimetallic nanocatalysts are superior to their monometallic counterparts in catalytic reactions, as exemplified by Pt–Co bimetallic nanoparticle catalysts in converting CO and H₂ into long-chain carbon fuels (Fischer–Tropsch synthesis) and in low-temperature fuel cell technologies.^{1–4} However, this additional degree of freedom introduces a new complexity in understanding reaction mechanisms, as the distribution of the two metal components may vary during reaction. For example, preferential adsorption of reactive molecules can induce phenomena such as the segregation of one component, changes in structure, as well as elemental-specific phase transformations.^{5–9} Because the structure of nanoparticles is flexible and can be modified drastically with environment, dealloying or realloying is inevitable during reactions and may eventually affect the catalytic performance.^{4,6,10,11} Uncovering the chemistry and structure of materials under reaction conditions is of fundamental importance in establishing structure–property relationships and to assist designing new catalytic materials.

Recent technical advances allow the characterization of nanoparticle catalysts while chemical reactions are proceeding. Ambient-pressure X-ray photoemission spectroscopy (AP-XPS) permits determination of the near surface structure and composition of bimetallic nanoparticles during reactions with various gases.⁹ The atomic structure of a single nanoparticle in

a fluid can also be observed directly using transmission electron microscopy (TEM).^{11–18} In addition, using molecular fluorescent markers in conjunction with optical microscopy it is possible to track the reaction products and surface chemistry of a single nanoparticle catalyst during liquid reactions.¹⁹ However, detailed atomic structural changes require a technique such as transmission electron microscopy, as both XPS and fluorescence microscopy do not provide atomic scale resolution. In order to address these questions, it is necessary to map the atomic structures in reactive environments *in situ*.

Here we use aberration-corrected environmental TEM to study Pt_{0.5}Co_{0.5} bimetallic nanoparticles during their reaction with O₂ and H₂ gases. The evolution of the atomic structure of the nanoparticles was captured in real time as the reaction was proceeding. The experiments were performed on a set of 10–12 nm Pt_{0.5}Co_{0.5} nanoparticles prepared by colloidal synthesis (Supporting Information). The nanoparticles were supported on an 8–12 nm thick silicon nitride membrane for TEM observation. The *in situ* experiments were carried out in the environmental TEM with postspecimen third order aberration

Received: February 11, 2014

Revised: April 18, 2014

correction operated at 300 keV with the $\pi/4$ phase plate tuned to >20 mrad prior to observation. A gas pressure range of 0.1–1 mbar was used during data acquisition where the temperature was at the 250–400 °C. A commercial Gatan furnace heating stage was used to heat the sample.

During oxidation at 250 °C in 0.1 mbar O₂ gas environment, Co segregates from the Pt–Co alloy nanoparticle and forms oxide on the surface, which is confirmed to be CoO via lattice spacing measurement. As shown in Figure 1a (also see

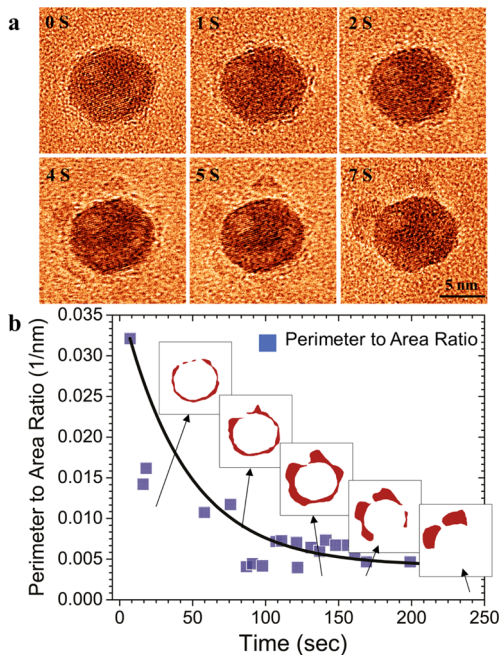


Figure 1. Atomic-scale reaction dynamics of a single Pt_{0.5}Co_{0.5} nanoparticle in an oxidizing environment (0.1 mbar O₂, 250 °C). (a) Sequential images of the particles during oxidation. (b) The quantification of the perimeter-to-area ratio of the segregated CoO phase as a function of time. The initial time in the label of in panel a is arbitrary. The sample was heated at 250 °C for 15 min before the images were taken to allow for sample stabilization.

Supporting Information Movie S1), the formation of CoO can be characterized as a two-stage process: (I) conformal coating and (II) island growth. The morphological evolution of CoO from stage (I) to stage (II) can be quantified using the perimeter-to-area ratio in the projected images (Figure 1b) that gives a semiquantitative description of both surface corrugation and the effective reaction surface of the particle. As shown in Figure 1b, after an initial period of 0–10 s (where a thin coating was observed) distinct CoO islands form on the nanoparticle surface. Correspondingly, the perimeter-to-area ratio decreases, indicating that the effective reaction surface per volume is reduced and the surface becomes rough. This is accompanied by the formation of vacancies that are inhomogeneously distributed in the interior of the particle. At a later point, these vacancies coalesce to form voids that are visible as lighter contrast areas in the images (Supporting Information Figure S1 and S2).

In order to identify the mechanisms of island growth, we analyzed a large number of nanoparticles during oxidation. Figure 2a shows sequential images of a Pt–Co nanoparticle during the early stage of phase segregation (Supporting Information Movie S2). Initially, Co atoms migrate to the

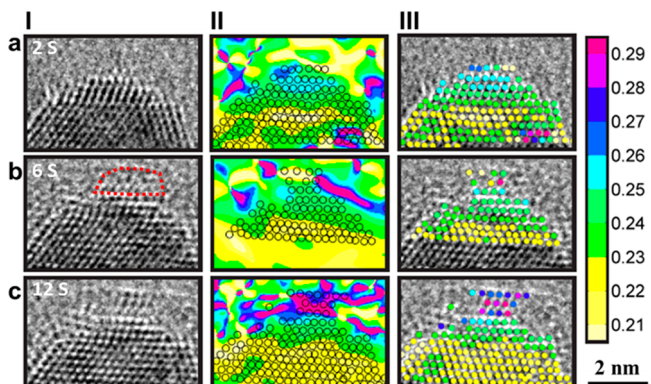


Figure 2. Tracking the atomic displacements during Co segregation in a single Pt_{0.5}Co_{0.5} nanoparticle under an oxidizing environment (0.1 mbar O₂, 250 °C). A series of images acquired at (a) 2 s, (b) 6 s, and (c) 12 s in situ during oxidation. Atomic resolution TEM images of the nanoparticle (column I). The atomic displacement maps of the nanoparticle shown by the color scale (from interlayer spacing measurements) suggests that the segregated Co forms a cubic CoO phase with expanding lattice (columns II and III).

surface of the Pt–Co nanoparticle and form CoO, as shown by the preserved atomic resolution images. The CoO is cubic with an epitaxial relationship with the host Pt–Co cubic lattice. Because of the large lattice mismatch between the two phases, the CoO lattice is compressively strained to fit on the lattice of Pt–Co.

The strain field and lattice relaxations were quantified with the well-established geometric phase analysis method (GPA)^{20–22} to map out the (111) interplane distance as a function of time and position (Supporting Information Figures S3 and S4). The strain maps obtained by GPA of sequential frames allow us to track the evolution of several components of the strain tensor at the atomic scale during the oxidation process. Figure 2(II) shows the strain field distribution corresponding to the images in Figure 2(I) (Supporting Information Figure S5). Colors represent the relative lattice displacements. At the initial stage (1 s), the area close to the top surface shows light blue or green corresponding to lattice spacing of 0.23–0.26 nm. This expansion is likely due to the incorporation of oxygen into the Pt–Co lattice, because the lattice is intact throughout the particle. Subsequently (at 6 s), a CoO island forms on top of the particle highlighted with a red dash line in Figure 2a. The island exhibits a larger lattice expansion as indicated by the light blue or red color. In contrast, the lattice in the bulk of the particle has a smaller lattice parameter as indicated by the dominant yellow color. After 12 s, when more CoO has segregated to the top surface, the strain map indicates a further expansion of the CoO lattice and a compression of the host lattice. It can be noted that the layer of oxide coating on the adjacent left side of the particle is very thin, and thus very limited lattice expansion is observed.

The detailed lattice spacing evolution for each atomic layer during phase segregation is plotted in Figure 3. Figure 3a shows a high-resolution TEM image of the interface between CoO and Pt–Co host lattice in the particle, with simulated crystal structures overlaid. The interfacial layer is labeled as “0”, the CoO atomic layers are “−1” to “−3” and the Co–Pt layers are “1” to “4”. The lattice displacements of each layer as a function of time (as measured from the GPA) are shown in Figure 3b, correspondingly, manual measurement of lattice spacing is

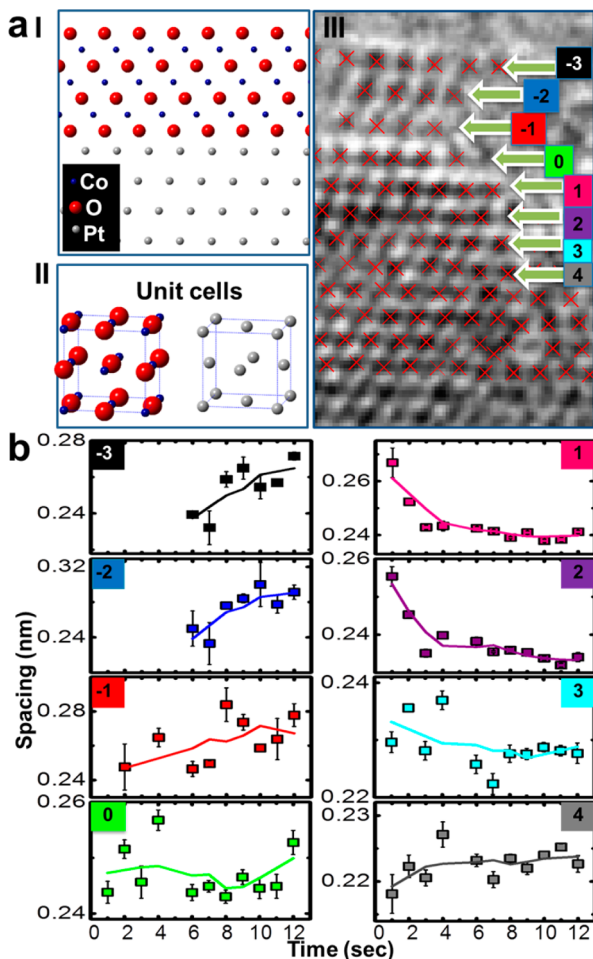


Figure 3. Evolution of lattice spacing of the atomic layers near the nanoparticle surface during oxidation. (a) (I) Schematic of the crystal structure at the interface between host Pt–Co lattice and CoO; (II) unit cells of Pt and CoO; (III) High-resolution image of the particle surface and of the interface between CoO and bulk Pt–Co. The arrows point at layers above (−1 to −3) and below (1 to 4) the interface. (b) Plot of the lattice spacing as a function of time for each layer. The expansion in CoO layers and the contraction of the Pt–Co layers-saturates after approximately 10 s.

performed in Supporting Information Figure S6 as well. There are minimal lattice changes in the interfacial layer, while the CoO lattice is compressed initially and it relaxes with time until it is saturated after about 10 s. This trend in the lattice changes can be explained as an initial oxygen deficiency resulting in a substoichiometric oxide film that reaches stoichiometry during an extended exposure to O₂. However, the decrease of the Pt–Co lattice spacing of layers “1” to “3” with time due to the outward diffusion of Co from the particle is counterintuitive. Normally, the reduced Co concentration in the Pt–Co alloy should result in an increase of lattice parameter, because Pt has larger lattice spacing than Co. Additionally, there are minimal lattice changes in the layer “4”, which is likely due to the limited Co outward diffusion within the time frame of experiments (~10 s). By comparing the lattice parameters of the layers “1” and “3” with that of inner layer “4”, we found the layers “1” and “3” have a larger lattice initially. This slight compressive lattice strain on Pt–Co lattice will increase the overlap between the metal d electrons on neighboring metal atoms.^{23–26} In order to keep the d occupancy fixed there will be a broadening of the d

bandwidth and a downshift of the d-band center (*ed*) with respect to the Fermi level. This would indicate a weaker chemisorption bond and reduced reactivity of the Pt-enriched particle surface.²³ The initial larger lattice of layers “1” to “3” can be simply explained by assuming that nucleation of CoO is the rate limiting step, due to the increased kinetic barrier of oxygen adsorption on the Pt-enriched particle surface. As a result, O can be adsorbed in the areas with Co-rich subsurfaces initially, giving rise to the larger lattice spacing.

The Co segregation process is reversible. Figure 4a shows low-angle annular dark-field scanning TEM (LAADF-STEM) images of the in situ reduction of Pt–Co nanoparticles that have been oxidized at 400 °C in 0.14 mbar of O₂. Prior to reduction (0 s), the cobalt oxide formed patches (highlighted in blue) surrounding the Pt-rich particles (yellow). As hydrogen reacts with the cobalt oxide, the cobalt oxide patches (blue area in Figure 4a) decrease. Formation of new particles was observed during reduction, which were identified to be metallic Co (Figure 4a, 241–503 s). These particles first grew larger and then shrunk and disappeared, a process that was accompanied by complementary changes of the Pt-rich particles. As shown in Figure 4a and in Supporting Information Figure S7, alloying of cobalt with these Pt-rich particles is associated with particle shape changes. These observations suggest that CoO on the surface is firstly reduced, and subsequently Co is reincorporated into Pt-rich lattice to form Pt–Co alloy particle.

To underpin the atomic-scale surface structure of the reduced particles, we performed an ex situ aberration-corrected STEM study of a set of Pt–Co particles that underwent an oxidation–reduction cycle. Those particles were treated at 400 °C in flowing dry air for 1.5 h, followed by a 400 °C treatment in flowing H₂. EELS mapping of the Co distribution within a reduced particle is shown in Figure 4c. This map demonstrates a significant contrast to the core–shell structure of the oxidized particles (Supporting Information Figure S8). The corresponding Co line profile across the particle suggests that the particle is solid. The chemical map also shows that the Co distribution is not completely uniform. This is in agreement with our in situ observations. In total, this indicates that heating to 400 °C was not sufficient to fully activate the alloying of these particles, thereby leaving some composition nonuniformity within the particle. A high-resolution ADF-STEM image (Figure 4b) shows the structure near the surface of the particles in the {111} orientation. Interestingly, the outermost atomic layer appears brighter than the layer underneath. Because the contrast in ADF-STEM images approximately scales with Z^{1.7}, this image strongly suggests that the {111} surface is Pt rich and the underlayer is Co rich.^{27,28}

The observation that Pt has segregated to the surface has important catalytic implications, especially for fuel cell applications.¹ Previous ex situ studies on Pt–Co systems have shown similar results. The number of layers of segregated Pt varies on different facets and it is dependent on the annealing temperature and gas pressure and generally varies between 1 and 3 layers.^{1,4,10,29} In our experiment specifically, this {111} single layer Pt segregation in H₂ is in contrast to the nearly complete segregation of Co in oxygen (Figure 2 versus Figure 4). This large difference in atomic-scale segregations can be attributed to the solubility/reaction of the ambient gas in/with the metal. A full understanding of this phenomenon requires further systematic explorations.

There are several factors that contribute to Co migration and phase segregation during the oxidation of Pt–Co in an O₂

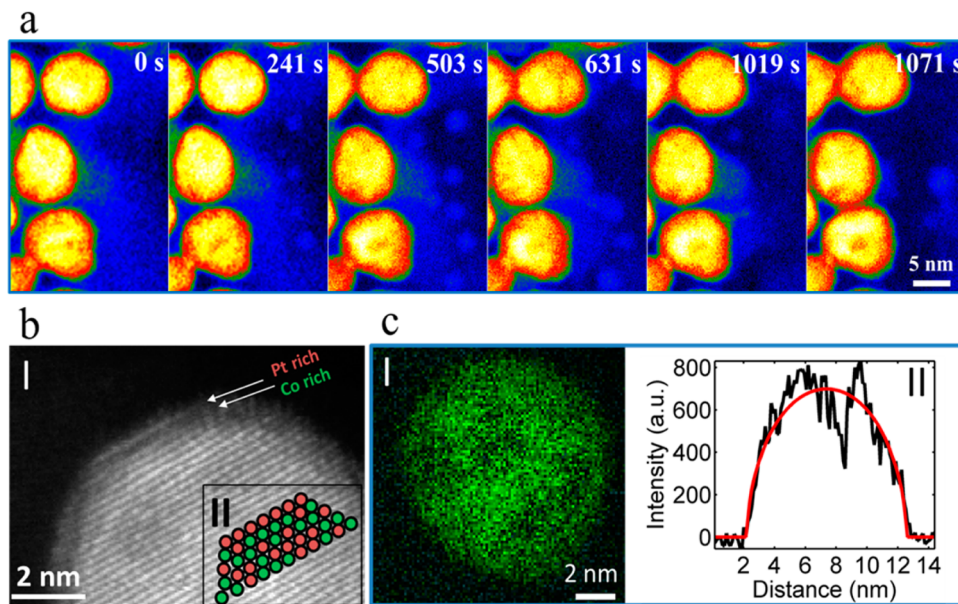


Figure 4. Atomic scale imaging and spectroscopy of the reduced Pt–Co nanoparticles. (a) Trajectory of the *in situ* reduction of oxidized Pt–Co nanoparticles. CoO are in blue and the metallic core is in yellow. (b) (I) Ex situ TEM image of the {111} surface of the Pt–Co nanoparticles after reduction showing a single layer of Pt segregation. The inset (II) is a schematic representation of the Co/Pt atoms distribution near the surface. (c) (I) The ex situ cobalt L-edge EELS map of a reduced Pt–Co particle showing that segregated cobalt has migrated back to the core. (II) Cobalt L-edge EELS intensity line profile across the particle overlaid with the line profile across a theoretically modeled particle.

atmosphere. First, because the Co–O bond is much stronger than the Pt–O bond, it is expected that the outermost layer of the nanoparticle will be composed of CoO. The solute oxygen may diffuse to Co/Pt or Co/Pt–Co interfaces through an interexchange mechanism.³⁰ Once oxygen reaches the Co/Pt–Co interface, the strong Co–O binding will favor the segregation of Co. Second, because the outward diffusion coefficients of Co are faster than inward diffusion of oxygen into the nanoparticle (Kirkendall effect) Co forms an oxide on the particle surface, creating a core–shell structure that leaves voids inside the particle. This is consistent with what was observed in Figure 1a. It is common that during a Kirkendall reaction the metallic species can diffuse through grain boundaries or other defects sites, and thus much faster diffusion than bulk diffusion through the lattice can be achieved.³¹ This is likely the case for the observed phase segregation. Additionally, because Co atoms are pulled out from the original Pt–Co structure during outward diffusion, the residual Pt atoms can form a monolayer underneath. Density function theory calculations suggest that the Pt layer is most stable in the second or third layer when there is sufficient oxygen over the outer layer. It is noted that during the reduction process the Co atoms diffuse back into the host particle, as shown in Figure 4. However, the driving force for this process is much weaker than the above Co segregation in O₂.^{32,33} As a result, Co atoms form a monolayer sandwiched by a Pt layer on the outermost surface and subsurface Pt–Co.

In conclusion, using a differentially pumped gas cell TEM we have observed the atomic scale details of the segregation of Co in Pt–Co bimetallic nanoparticles in oxidizing environments and the reabsorption of Co in reducing environments. The ability to observe atomic scale details of the evolution of the structure of nanoparticles in their reactive environments opens the way to a deeper understanding of the heterogeneous catalysis. It also allows for the study of a wider variety of nanoparticle systems where reaction pathways remain elusive.

■ ASSOCIATED CONTENT

S Supporting Information

Material and Methods, Figures S1-S-8, Movies S1 and S2, and movie captions. This material is available free of charge via the Internet at <http://pubs.acs.org>.

■ AUTHOR INFORMATION

Corresponding Author

*E-mail: hmzheng@lbl.gov.

Notes

The authors declare no competing financial interest.

■ ACKNOWLEDGMENTS

Part of *in situ* environmental TEM experiments was carried out at William R. Wiley Environmental Molecular Sciences Laboratory (EMSL), a national scientific user facility sponsored by the U.S. Department of Energy (DOE) Office of Biological and Environmental Research and located at Pacific Northwest National Laboratory (PNNL). PNNL is operated by Battelle for DOE under Contract DE-AC05-76RLO1830. Part of the *in situ* work was conducted at the Center for Functional Nanomaterials (CFN), Brookhaven National Laboratory (BNL), which is supported by the DOE Office of Basic Sciences (BES), under Contract No. DE-AC02-98CH10886. We thank Dr. James Ciston and Rosa E. Diaz for their help during the initial data acquisition at BNL. We performed *ex situ* TEM experiments at National Center for Electron Microscopy (NCEM) of the Lawrence Berkeley National Laboratory (LBNL), which is supported by the DOE BES under Contract No. DE-AC02-05CH11231. H.L.X. was supported by SERC at LBNL. C.M.W. and L.K. were supported by the Chemical Imaging Initiative at PNNL, which was under the Laboratory Directed Research and Development Program at PNNL. M.S. was supported by the Office of Basic Energy Sciences, Chemical Science Division of the U.S. DOE under Contract No. DE-

AC02-05CH11231. R.T. is supported by H.Z.'s Early Career Research Program under the DOE Office of Science. H.Z. was a residency faculty of SinBeRise program of BEARS at University of California, Berkeley during July 2013–Jan. 2014.

(33) Herron, J.; Mavrikakis, M. *Catal. Commun.* **2013**, In Press.

■ REFERENCES

- (1) Stamenkovic, V. R.; Mun, B. S.; Arenz, M.; Mayrhofer, K. J. J.; Lucas, C. A.; Wang, G.; Ross, P. N.; Markovic, N. M. *Nat. Mater.* **2007**, 6 (3), 241–247.
- (2) Schanke, D.; Vada, S.; Blekkan, E. A.; Hilmen, A. M.; Hoff, A.; Holmen, A. *J. Catal.* **1995**, 156 (1), 85–95.
- (3) Vada, S.; Hoff, A.; Adnanes, E.; Schanke, D.; Holmen, A. *Top. Catal.* **1995**, 2 (1–4), 155–162.
- (4) Wang, D.; Xin, H. L.; Hovden, R.; Wang, H.; Yu, Y.; Muller, D. A.; DiSalvo, F. J.; Abruña, H. D. *Nat. Mater.* **2013**, 12 (1), 81–87.
- (5) Hansen, P. L.; Wagner, J. B.; Helveg, S.; Rostrup-Nielsen, J. R.; Clausen, B. S.; Topsøe, H. *Science* **2002**, 295 (5562), 2053–2055.
- (6) Wang, D.; Xin, H. L.; Yu, Y.; Wang, H.; Rus, E.; Muller, D. A.; Abruna, H. D. *J. Am. Chem. Soc.* **2010**, 132 (50), 17664–17666.
- (7) Zheng, F.; Alayoglu, S.; Guo, J.; Pushkarev, V.; Li, Y.; Glans, P.-A.; Chen, J.-I.; Somorjai, G. *Nano Lett.* **2011**, 11 (2), 847–853.
- (8) Newton, M. A.; Belver-Coldeira, C.; Martinez-Arias, A.; Fernandez-Garcia, M. *Nat. Mater.* **2007**, 6 (7), 528–532.
- (9) Tao, F.; Grass, M. E.; Zhang, Y.; Butcher, D. R.; Renzas, J. R.; Liu, Z.; Chung, J. Y.; Mun, B. S.; Salmeron, M.; Somorjai, G. A. *Science* **2008**, 322 (5903), 932–934.
- (10) Xin, H. L.; Mundy, J. A.; Liu, Z.; Cabezas, R.; Hovden, R.; Kourkoutis, L. F.; Zhang, J.; Subramanian, N. P.; Makharia, R.; Wagner, F. T.; Muller, D. A. *Nano Lett.* **2011**, 12 (1), 490–497.
- (11) Liao, H.-G.; Cui, L.; Whitelam, S.; Zheng, H. *Science* **2012**, 336 (6084), 1011–1014.
- (12) Yoshida, H.; Kuwauchi, Y.; Jinschek, J. R.; Sun, K.; Tanaka, S.; Kohyama, M.; Shimada, S.; Haruta, M.; Takeda, S. *Science* **2012**, 335 (6066), 317–319.
- (13) Tao, F.; Salmeron, M. *Science* **2011**, 331 (6014), 171–174.
- (14) Gai, P.; Boys, E. D. *14th European Microscopy Congress* **2008**, 479–480.
- (15) Dubau, L.; Dursta, J.; Maillard, F.; Guétazb, L.; Chateneta, M.; Andréc, J.; Rossinotc, E. *Electrochim. Acta* **2011**, 56, 16.
- (16) Carlton, C. E.; Chen, S. C.; Ferreira, P. J.; Allard, L. F.; Yang, S.-H. *J. Phys. Chem. Lett.* **2012**, 3 (2), 161–166.
- (17) Yu, Y.; Xin, H.; Hovden, R.; Wang, D.; Rus, E. D.; Mundy, J. A.; Muller, D. A.; Abruña, H. D. *Nano Lett.* **2012**, 12 (9), 4417–4423.
- (18) Gai, P.; Sharma, R.; Ross, F. *MRS Bull.* **2008**, 33 (2), 107–114.
- (19) Xu, W.; Kong, J. S.; Yeh, Y.-T. E.; Chen, P. *Nat. Mater.* **2008**, 7 (12), 992–996.
- (20) Hýtch, M. J. *Ultramicroscopy* **1998**, 74 (3), 131–146.
- (21) Hýtch, M. J. *Nature* **2003**, 423, 270–273.
- (22) Pratt, A.; Lari, L.; Hovorka, O.; Shah, A.; Woffinden, C.; Tear, S.; Binns, C.; Kroger, R. *Nat. Mater.* **2013**, 13, 26–30.
- (23) Kitchin, J.; Korskov, J.; Barreau, M.; Chen, J. *Phys. Rev. Lett.* **2004**, 93, 15.
- (24) T, B. *Electrochim. Acta* **2007**, 52.
- (25) Qiu, H.; Zou, F. *Appl. Mater. Interfaces* **2012**, 4 (3), 1404–1410.
- (26) Zhang, X.; Wang, H.; Key, J.; Linkov, V.; Ji, S.; Wang, X.; Lei, Z.; Wang, R. *J. Electrochem.* **2012**, 159 (3), 8270–8276.
- (27) Zheng, F. A.; Selim. *Catal. Today* **2011**, 182 (1), 54–59.
- (28) Alayoglu, S.; Beaumont, S. K.; Zheng, F.; Pushkarev, V. V.; Zheng, H.; Iablokov, V.; Liu, Z.; Guo, J.; Kruse, N.; Somorjai, G. A. *Top. Catal.* **2011**, 54 (13–15), 778–785.
- (29) Chen, S.; Sheng, W.; Yabuuchi, N.; Ferreira, P. J.; Allard, L. F.; Shao-Horn, Y. *J. Phys. Chem. C* **2008**, 113 (3), 1109–1125.
- (30) Lanyon, M. A. H.; Trapnell, B. M. W. *Proc. R. Soc. London, Ser. A* **1955**, 227 (1170), 387–399.
- (31) Niu, K.-Y.; Park, J.; Zheng, H.; Alivisatos, P. *Nano Lett.* **2013**, 13 (11), 5715–5719.
- (32) Xu, Y.; Ruban, A. V.; Mavrikakis, M. *J. Am. Chem. Soc.* **2004**, 126 (14), 4717–4725.